Journal of Nanobiotechnology

RESEARCH

Open Access

Metal ions-anchored bacterial outer membrane vesicles for enhanced ferroptosis induction and immune stimulation in targeted antitumor therapy

Ying Sun[1†], Yan-Yan Ma[1†], Shijie Shangguan[2†], Yihang Ruan[2,3], Tingjie Bai[2], Panpan Xue[2], Huilan Zhuang[2], Wenyu Cao[1], Huimei Cai[1*], Enqi Tang[1], Zhou Wu[1], Mingzhen Yang[1], Yixin Zeng[1], Juan Sun[1], Yong Fan[1], Xuemei Zeng[3] and Shuangqian Yan[2*]

Abstract

The activation of ferroptosis presents a versatile strategy for enhancing the antitumor immune responses in cancer therapy. However, developing ferroptosis inducers that combine high biocompatibility and therapeutic efficiency remains challenging. In this study, we propose a novel approach using biological nanoparticles derived from outer membrane vesicles (OMVs) of *Escherichia coli* for tumor treatment, aiming to activate ferroptosis and stimulate the immune responses. Specifically, we functionalize the OMVs by anchoring them with ferrous ions *via* electrostatic interactions and loading them with the STING agonist-4, followed by tumor-targeting DSPE-PEG-FA decoration, henceforth referred to as OMV/SaFeFA. The anchoring of ferrous ions endows the OMVs with peroxidase-like activity, capable of inducing cellular lipid peroxidation by catalyzing H_2O_2 to $^{\bullet}OH$. Furthermore, OMV/SaFeFA exhibits pH-responsive release of ferrous ions and the agonist, along with tumor-targeting capabilities, enabling tumor-specific therapy while minimizing side effects. Notably, the concurrent activation of the STING pathway and ferroptosis elicits robust antitumor responses in colon tumor-bearing mouse models, leading to exceptional therapeutic efficacy and prolonged survival. Importantly, no acute toxicity was observed in mice receiving OMV/SaFeFA treatments, underscoring its potential for future tumor therapy and clinical translation.

Keywords Ferroptosis, Bacterial outer membrane vesicle, STING, Immunotherapy

†Ying Sun, Yan-Yan Ma and Shijie Shangguan contributed equally to this work.

*Correspondence:
Huimei Cai
Cai_Fzsy@163.com
Shuangqian Yan
ifeshqyan@fjnu.edu.cn

[1]Department of Gastroenterology, Fuzhou No. 1 Hospital Affiliated with Fujian Medical University, Fuzhou, Fujian 350009, China
[2]Straits Laboratory of Flexible Electronics (SLoFE), Straits Institute of Flexible Electronics (SIFE, Future Technologies), Fujian Normal University, Fuzhou, Fujian 350117, China
[3]Key Laboratory of Microbial Pathogenesis and Interventions of Fujian Province University, Biomedical Research Center of South China, College of Life Sciences, Fujian Normal University, Fuzhou, Fujian 350117, China

Introduction

Ferroptosis, characterized by iron-mediated reactive oxygen species (ROS) generation leading to lipid peroxidation (LPO) and subsequent membrane rupture, has garnered significant attention in various applications, particularly in tumor treatments, over the past decade [1–5]. The cellular enrichment of iron ions and ROS accumulation are believed to promote ferroptosis [6, 7]. However, the effectiveness of LPO may be hindered by intrinsic cellular defense mechanisms, such as the selenium-dependent cyst(e)ine-glutathione (GSH) peroxidase 4 (GPX4)-GSH axis [8]. Cystine, imported by the cystine/glutamine antiporter solute carrier family 7 member 11 (SLC7A11 or system Xc^-), contributes to GSH biosynthesis, which serves as both an antioxidative substrate for ROS elimination and a cofactor for GPX4 [9]. GPX4 converts lethal phospholipid hydroperoxides to harmless lipid alcohols, thus inhibiting ferroptosis. Consequently, inhibiting SLC7A11 can induce ferroptosis in cancer cells. While various small molecules have been employed to target SLC7A11, their poor pharmacokinetics and lack of tumor-targeting often result in unsatisfactory therapeutic outcomes and unwanted side effects. Interestingly, interferon-γ (IFN-γ), secreted by activated immune cells, can suppress SLC7A11 to promote ferroptotic cell death, while ferroptosis itself can activate the body's antitumor immune responses [10–12]. Therefore, combining ferroptosis with immunotherapy represents a potent approach for tumor treatments [13, 14].

Nanoparticle-based delivery systems have found extensive application in delivering inducers or immune modulators for tumor ferroptosis and immunotherapy [15–17]. This is attributed to their ability to enhance the pharmacokinetics and tumor-targeting of therapeutics through the enhanced permeability and retention effect. Additionally, many types of nanoparticles possess biological enzyme mimicking properties, referred to as nanozymes, which enable tumor-specific catalytic treatments and potentiate ferroptosis [18–21]. For example, nanoparticles exhibiting peroxidase (POD)-like activity, such as metallic oxides and metal-organic frameworks, can catalyze the conversion of tumoral H_2O_2 to ROS, thereby inducing cellular ferroptosis [22–24]. Furthermore, GSH oxidase-like materials can disrupt the cyst(e)ine-GPX4-GSH axis by depleting GSH, thus enhancing ferroptosis in cancer cells [25]. These nanoparticles often elicit antitumor immune responses through ferroptosis-evolved immunogenic cell death or in combination with immune modulation factors and checkpoint blockers [26–28]. However, the synthetic processes of nanoparticles are intricate, and their components are often clinically unavailable, leading to potential biotoxicity and challenges in clinical translation [7].

Biological nanoparticles derived from natural sources, including plants, fruits, eukaryotes, and prokaryotes, hold significant promise for therapeutic delivery in tumor treatments owing to their inherent biocompatibility and functionality [29–31]. For example, outer membrane vesicles (OMVs) produced by gram-negative bacteria have garnered attention for their tumor-targeting capabilities, biocompatibility, engineering potential, and immune-modulating properties [32–34]. OMVs can be functionalized through genetic engineering of the parent bacteria, post-chemical modification, or direct drug loading, enabling tumor modulation through various therapeutic approaches [35, 36]. Despite these advantages, OMVs have yet to be explored for eliciting tumor ferroptosis. Moreover, the complex and immunosuppressive nature of the tumor microenvironment necessitates high OMV doses for immune activation, potentially leading to side effects due to their inherent toxin components [37, 38]. Therefore, there is an urgent need to employ OMVs safely to enhance immune responses and explore their application in ferroptosis induction.

In light of the context outlined above, we propose to engineer OMV for tumor-targeted combinational ferroptosis and immunotherapy by imparting it with POD-like activity and loading immune adjuvants. OMV was selected based on its inherent biocompatibility and functionality, rendering it a suitable candidate for the drug delivery system. Specifically, OMV are loaded with stimulator of interferon genes (STING) agonist-4 followed by Fe^{2+} ion absorption. STING agonists are selected for their ability to activate the STING pathway, which enhances innate and adaptive immunity efficaciously for tumor treatment [39, 40]. This augmented immunity fosters the production of IFN-γ by T cells, particularly $CD8^+$ cells, which enhances cellular ferroptosis by inhibiting SLC7A11 [10]. Cationic Fe^{2+} ions are absorbed by negatively charged OMVs *via* electrostatic interaction. Consequently, the ion-absorbed OMVs (OMV/Fe) not only deliver Fe^{2+} into cells but also inherit the POD-like activity of Fe^{2+}, resulting in cellular accumulation of ROS and LPO. Furthermore, given the high expression of folate receptor on MC38 colon tumor cells, the folate-anchored DSPE-PEG-FA was incorporated into OMV/SaFe to enhance the tumor-targeting abilities of OMV. Upon systemic injection, the prepared OMV/SaFeFA induces tumor ferroptosis and robust antitumor responses without evident side effects in a mouse colon tumor model (Scheme 1).

Materials and methods

Chemicals and reagents

Copper chloride, iron(II) chloride, manganese chloride, zinc nitrate, cobalt nitrate hexahydrate, vitamin E, Ferrostatin-1 (Fer-1), and propidium iodide (PI) were

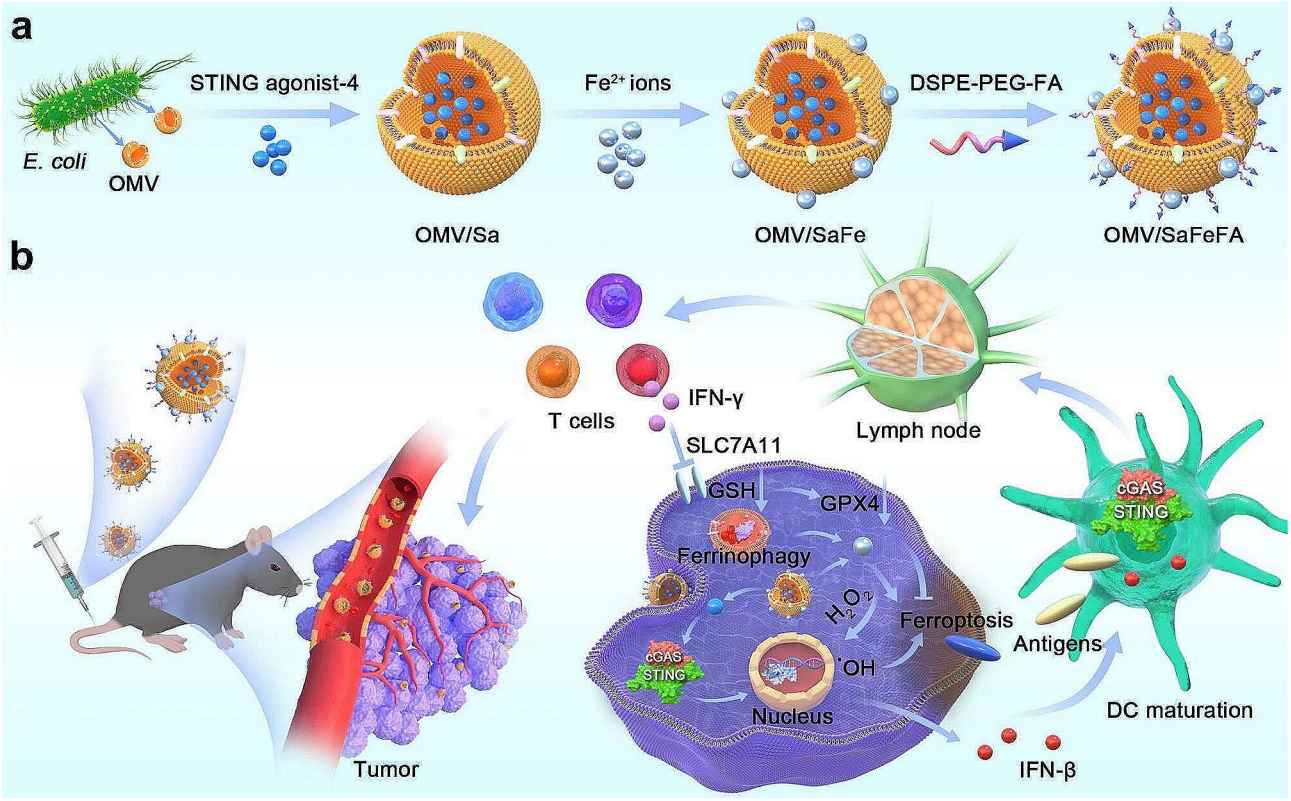

Scheme 1 (**a**) Preparation process of OMV/SaFeFA by engineering outer membrane vesicles (OMVs) derived from *Escherichia coli*. (**b**) Schematic illustration of OMV/SaFeFA for tumor ferroptosis activation and antitumor immune response elicitation

procured from Shanghai Aladdin Biochemical Technology Co., Ltd. 3-Methyladenine (3-MA) was got from Shanghai Maclin Biochemical Technology Co., Ltd. Hydrochloric acid (HCl) was purchased from Sinopharm. Z-VAD-FMK, the reactive oxygen species (ROS) kit, 2-(4-amidinophenyl)-6-indolecarbamidine dihydrochloride (DAPI), Annexin V-FITC apoptosis kit, and Calcein-AM were obtained from Beyotime Biotechnology. Liperfluo was received from Dojindo. CCK-8 kit was got from Sangon Biotechnology. 3,3′,5,5′-tetramethylbenzidine (TMB) solution (1%) was bought from Solarbio. STING agonist-4 was received from Invivochem. PE anti-mouse CD8a antibody (Cat#100708), FITC anti-mouse CD4 antibody (Cat#116003), APC anti-mouse CD3 antibody (Cat#152306), PE anti-mouse CD86 antibody (Cat#105008), FITC anti-mouse CD80 antibody (Cat#104706), and APC anti-mouse CD11c antibody (Cat#117310) were bought from Biolengend. Anti-CALR antibody (A00894-1) and goat anti-rabbit IgG(H+L) (AF594 conjugated, E-AB-1060) were obtained from Boster biological technology and Elabscience, respectively. Dulbecco's Modified Eagle Medium (DMEM) was purchased from Hyclone. Fetal bovine serum (FBS) was got from Gibco. Penicillin-streptomycin was bought from BasalMedia. Phosphate buffer (PBS) was bought from Sigma. DEPE-PEG-FA and DEPE-PEG (MW 2000) were obtained from AVANTI.

Instruments

3,3′,5,5′-tetramethylbenzidine (TMB) absorbance was measured using a microplate reader (Thermofisher, Multiskan Sky). Fluorescent images were acquired using a laser scanning confocal microscope (Zeiss, LSM 780). Zeta potential and hydrodynamic size were performed by ZS90 (Zetasizer Nano, Malvern). TEM images were captured using a Hitachi HT7700 transmission electron microscopy. Flow cytometry analysis was performed using FACSymphony™ A5, BD Bioscience.

OMV purification and functionalization

OMV was obtained by ultracentrifugation of DH-5α culture supernatant. Briefly, DH-5α was cultured in Luria-Bertani medium for 16 h at 200 rpm shaking speed at 37 °C. Then, bacterial cells were removed by centrifugation at 4000 g for 20 min at 4 °C. The obtained supernatant was further filtered by 0.45 μm membrane filters to remove large bacterial debris. Following this, the supernatant was centrifuged at 30,000 rpm for 2.5 h at 4 °C. The resulting precipitate was resuspended in 500 μL PBS and stored at -20 °C for the subsequent experiments. Total protein concentration was quantified using a

bicinchoninic acid (BCA) kit, defining the concentration as the OMV concentration.

To form OMV/Fe composites, 1.4 mL OMV (4.2 mg/mL) was mixed with 200 μL metal salts (with a concentration of 1.2 mg/mL) for 2 h at 4 °C using a rotary mixer. The mixture was then centrifuged at 14,000 rpm for 0.5 h at 4 °C, and the resulting precipitate was re-suspended in 1 mL PBS.

For the fabrication of OMV/SaFeFA, 6 mg OMV was first stirred with 1 mg STING agonist-4 for 8 h at 4 °C. Subsequently, $FeCl_2$ solution (2 mg) was slowly dropped into the above mixture under vigorous shaking. After 2 h, 3 mg DSPE-PEG-FA was added for another 1 h. Last, the precipitate was got under centrifugation at 4 °C (14000 rpm, 30 min). The resulting OMV/SaFeFA was resuspended in PBS and stored at -20 °C.

The DSPE-PEG was escorted into prepared OMV to get DSPE-PEG modified OMV (OMV-PEG) by simply co-incubation [41]. Similar procedures were used to obtain DSPE-PEG-FA-modified OMV (OMV/FA), Fe-anchored OMV/FA (OMV/FeFA), STING agonist-4-loaded OMV/FA (OMV/SaFA), DSPE-PEG-modified OMV (OMV-PEG), Cyanine 5 (CY5)-loaded OMV-PEG (OMV/CY5-PEG), CY5-loaded OMV/FA (OMV/CY5-PEG-FA), and CY5-loaded OMV/FeFA (OMV/CY5FeFA).

$^{\cdot}OH$ detection

OMV/ions (50 μL) were mixed with 100 μL TMB and 5 μL 0.03% H_2O_2 solutions at room temperature. After 10 min, the reaction was terminated by 155 μL HCl (1 M), and the absorbance at 450 nm was recorded by a microplate reader.

Characteristic protein of OMVs profiles

5 μg OMV or OMV/Fe were mixed with loading buffer, boiled 10 min, and then subjected to 10% sodium dodecyl sulfate-polyacrylamide gel electrophoresis (SDS-PAGE). After electrophoresis, proteins of OMVs were visualized by Coomassie brilliant blue staining for 30 min and analyzed using a gel imaging system (JS-6800).

Release behavior assay

OMV/SaFeFA was prepared and incubated in buffer solutions of varying pH values for different durations (0, 1, 2, 4, 8, and 12 h). Subsequently, the samples were centrifuged at 14,000 rpm for 10 min, and the supernatant was collected to assess the levels of STING agonist and Fe^{2+} ions. The STING agonist level was determined by measuring the UV-vis spectra absorbance at 320 nm, while the Fe^{2+} ion level was evaluated using phenanthroline spectrophotometry.

Cell culture

MC38 and 4T1 cells were cultured in DMEM media supplemented with 10% FBS and 1% streptomycin/penicillin and maintained in a cell incubator at 37 ℃ with 5% CO_2. DC2.4 cells were cultured in RPMI-1640 media supplemented with 10% FBS, 1% streptomycin/penicillin, and maintained in a cell incubator at 37 ℃ with 5% CO_2.

Cell uptake

MC38 cells (1×10^6) were seeded in 6-well plates and cultured overnight. Next, OMV/CY5FeFA solution (OMV: 40 μg/mL, CY5: 20 μg/mL) was co-cultured with MC38 cells for various duration (5 min, 2 h, 4 h, 8 h, and 12 h). Finally, cells samples were collected and analyzed using flow cytometry.

CCK-8 assay

MC38 cells (5000) were seeded in 96-well plates and cultured overnight. Next, PBS, OMV/FA, OMV/FeFA, OMV/SaFA, and OMV/SaFeFA were added to the cell culture medium at concentrations of 15 μg/mL for OMV and 7.5 μg/mL for STING agonist-4. After 24 h, cell viability was assessed using a CCK-8 kit.

To explore the cell death pathway, MC38 cells (5000) were seeded in 96-well plates and cultured overnight. Then, cell samples were co-incubated with OMV/SaFeFA and various inhibitors (Fer-1: 2 μM; vitamin E: 20 μM; and 3-MA: 10 μM). Subsequently, cell viability was determined using a CCK-8 kit.

To investigate the effect of concentration on cell viability, MC38 cells (5000) were seeded in 96-well plates and cultured overnight. Then, the cell samples were cultured with various concentrations of OMV/SaFeFA (2.5, 5, 7.5, 10, 15, and 20 μg/mL, total protein concentration was defined to be the OMV/SaFeFA concentration) for 24 h. Following incubation, the cell viability was assessed using a CCK-8 kit.

Intracellular Fe^{2+} imaging

MC38 cells were seeded in confocal dishes and cultured overnight. Thereafter, the cells were incubated with OMV/SaFeFA for various time points (0, 2, 4, 8, and 12 h). After incubation, the cell samples were washed three times with PBS and then stained with FerroOrange fluorescent probes for 30 min. The fluorescent signals of cell samples were observed by a confocal laser scanning microscopy (CLSM).

ROS and $^{\cdot}OH$ imaging

MC38 cells (1×10^5) were seeded in confocal small dishes and cultured overnight. Then, PBS, OMV/FA, OMV/FeFA, OMV/SaFA, OMV/SaFeFA, H_2O_2 (200 μM), and OMV/SaFeFA + H_2O_2 (200 μM) were added into the cell culture medium. The concentrations of OMV and STING

agonist-4 were 15 and 7.5 μg/mL, respectively. After 24 h, the cells were stained with the DCFH-DA (ROS fluorescent probe) and BboxiProbe O26 (•OH fluorescent probe) according to the manufacturer protocols and imaged by a CLSM. The fluorescent intensity of the images was measured by an Image J software.

Ferroptosis study

MC38 cells (1×10^5) were seeded in confocal small dishes and cultured overnight. Subsequently, PBS, OMV/FA, OMV/FeFA, OMV/SaFA, OMV/SaFeFA, and $FeCl_2$ (30 μg/mL) were added to the cell culture medium. The concentrations of OMV and STING agonist-4 were 15 and 7.5 μg/mL, respectively. Following a 24-h incubation period, cells were stained with the Liperfluo probe according to the manufacturer's protocols and imaged using a CLSM.

Apoptosis analysis

MC38 cells (1×10^6) were seeded in 6-well plates and cultured overnight. Then, PBS, OMV/FA, OMV/FeFA, OMV/SaFA, and OMV/SaFeFA were added into the cell culture medium. After 24 h, cells were harvested and stained with Annexin V-FITC and PI. The apoptosis of cells was analyzed using flow cytometry.

CRT staining

MC38 cells (1×10^5) were seeded in confocal small dishes and cultured overnight. Afterward, cells were co-incubated with PBS, OMV/FA, OMV/SaFA, OMV/FeFA, and OMV/SaFeFA for 24 h. Following incubation, the cells were fixed with 4% paraformaldehyde for 30 min, and then stained with anti-CALR antibody (1: 200) for 30 min. After washing three times with PBS, the cells were incubated with goat anti-rabbit IgG(H+L) (AF594 conjugated, 1: 100) for 30 min. Finally, the cells were counterstained with DAPI and imaged using a CLSM.

Western blot assay

MC38 cells (1×10^6) were seeded in 6-well plates and cultured overnight. Then, PBS, OMV/FA, OMV/SaFA, OMV/FeFA, and OMV/SaFeFA were added into the cell culture medium. After 24 h, cells samples were collected and processed following standard western blot protocols.

In vitro activation of STING pathway

MC38 cells and DC 2.4 cells were seeded in 6-wells plates and cultured overnight. MC38 cells were incubated with PBS, OMV/FA, OMV/FeFA, OMV/SaFA, and OMV/SaFeFA for 24 h. Afterward, the supernatants were collected and incubated with DC 2.4 cells for another 24 h. The treated DC 2.4 cells were then lysed in radioimmunoprecipitation assay (RIPA) buffer with protease inhibitors. For western blot analysis, 15 μg of whole cell lysates were mixed with loading buffer, boiled for 10 min, and subjected to 10% SDS-PAGE at 80 V for 20 min followed by 120 V 60 min. The proteins were then transferred onto a polyvinylidene fluoride membrane, which was subsequently blocked for 1 h in 5% non-fat milk. The membrane was then incubated overnight at 4 ℃ with an anti-STING antibody. Immunoreactive protein was visualized using a recommended dilution of conjugated secondary antibody, and the luminescent bands were visualized by Automatic Gel Imaging Analyzer, JS-6800. The concentration of IFN-β in the supernatants of DC 2.4 cells was measured using a commercial kit.

Biodistribution

All mouse experiments were implemented in accordance with protocols approved by the Animal Experimental Ethics Committee of the Fujian Normal University (No. IACUC-20220005). C57/BL6 and BALB/c mice (4–6 weeks) were sourced from Beijing Hua Fu Kang Biotechnology Co., ltd. Nine MC38 tumor-bearing C57/BL6 mice were randomly divided into 3 groups. Mice were i.v. injected with CY5, OMV/CY5-PEG, and, OMV/CY5-PEG-FA, with CY5 and OMV doses set at 50 μg and 60 μg, respectively. Then, the fluorescent signals of mice were recorded at different time points (20 min, 2 h, 4 h, 8 h, 10 h, and 24 h) using an IVIS system. After 24 h, mice were euthanized, and the fluorescent signals of tumors and major organs were recorded.

For the 4T1 breast tumor model, nine tumor-bearing BALB/c mice were randomly allocated into 3 groups. These mice received i.v. injection of CY5, OMV/CY5-PEG, and, OMV/CY5-PEG-FA. At 24 h post-injection, mice were euthanized, and the fluorescent signals of tumors and major organs were recorded. Fluorescence images of tumor slices were captured using a CLSM.

In vivo therapy

C57/BL6 mice received an injection of 1×10^6 MC38 cells in the right hind leg flank. Ten days later, the MC38 tumor-bearing mice were randomly divided into 5 groups ($n=4$) and i.v injected with PBS, OMV/FA, OMV/SaFA, OMV/FeFA, and OMV/SaFeFA on days 0 and 4. Tumor size and body weight were measured every two days throughout the treatment period, with tumor volumes calculated using the formula: $V= (\text{length} \times \text{width}^2)/2$. On day 16, mice were euthanized, and the tumors were collected. Tumors were weighted, sliced, and analyzed for H&E, TUNEL staining, and immunohistochemical staining of IFN-γ, SLC7A11, GPX4, NCOA4, and FTH1. Serum was collected for IFN-γ detection using a commercial kit. In addition, the long-term survival rates were evaluated by the same procedures except for monitoring 58-day period.

Biosafety

PBS, OMV/FA, OMV/FeFA, OMV/SaFA, and OMV/SaFeFA were administered *via* the tail vein of C57/BL6 mice. After a 16-day treatment, blood samples from C57/BL6 mice were collected for biochemical analysis. The parameters measured included blood urea nitrogen (BUN), aspartate aminotransferase (AST), alanine aminotransferase (ALT), and alkaline phosphatase (ALP), and gamma glutamyl transpeptidase (γ-GT), using assay kits from Solarbio (BC1555, BC1535, BC2145, BC1565, and BC1225). Subsequently, mice were sacrificed, and the major organs (heart, liver, spleen, lung, and kidney) were harvested and subjected to H&E staining for histological analysis.

Immune response analysis

MC38 bearing tumor-bearing mice were randomly divided into 5 groups ($n=3$) and i.v injected with PBS, OMV/FA, OMV/SaFA, OMV/FeFA, and OMV/SaFeFA on days 0 and 4. After 16-day treatment, mice were euthanized, and tumors were collected and made to single-cell suspensions through 40 μm nylon mesh filters. Subsequently, the cell samples were stained with designated fluorescent antibodies and analyzed using flow cytometry.

Statistical analysis

Quantitative data were presented as mean ± standard error of the mean (SEM). All experiments were repeated three times or more. Statistics were analyzed by one-way ANOVA, followed by Dunnett's multiple comparisons test using GraphPad Prism 8.0. Statistical significance was denoted by an asterisk. P values of 0.05 or less were considered statistically significant (ns: not significant, $^{*}p<0.05$, $^{**}p<0.01$, $^{***}p<0.001$, and $^{****}p<0.0001$).

Results and discussion

OMV engineering and characterization

OMV was obtained by ultracentrifugation of DH-5α culture supernatant according to the previous report [32]. Then, we conducted a cation screening for OMV absorption through simple stirring. After mixing with various cations (Zn^{2+}, Cu^{2+}, Fe^{2+}, Ni^{2+}, Co^{2+}, and Mn^{2+}), the OMV was centrifuged at moderate speed of 14,000 rpm (Fig. 1a), indicating successful modification with all cations. Notably, according to the results of 3,3',5,5'-tetramethylbenzidine (TMB) oxidation assay, OMV/Fe^{2+} exhibited the highest catalytic activity among the ion-decorated OMV in the presence of H_2O_2, with the fold enhancement of TMB reaching approximately 38 (Fig. 1b and c and S1). Interestingly, the absorbance of TMB-treated OMV/Mn^{2+} in the presence of H_2O_2 decreased compared the mixture without H_2O_2, which may arise from the superoxide dismutase-mimicking activity of the Mn^{2+} ion [42]. Thus, we selected Fe^{2+}-modified OMV for subsequent experiments owing to its excellent Fenton activity for tumor catalytic therapy. Coomassie brilliant blue staining results indicated that the band patterns of OMV/Fe^{2+} was identical to those of OMV, suggesting that Fe^{2+} modification had no obvious impact on the proteins (Figure S2). To further enhance tumor-targeting ability, we modified OMV with DSPE-PEG-FA, denoted as OMV/FA, to target folate receptors that overexpressed on most tumor cell lines. Transmission electron microscopy (TEM) analysis revealed that OMV modified with DSPE-PEG-FA (OMV/FA), DSPE-PEG-FA and Fe^{2+} (OMV/FeFA), DSPE-PEG-FA and STING-agonist (OMV/SaFA) and DSPE-PEG-FA, Fe^{2+}, and STING-agonist (OMV/SaFeFA) exhibited spherical morphologies and were almost the same size as OMV (Fig. 1d). The SA can be loaded inside the OMV lumen [43] and Fe^{2+} can be absorbed onto the surface of OMV [44]. Additionally, DSPE-PEG-FA was incorporated into the prepared OMV to produce DSPE-PEG modified OMV (OMV-PEG) through simple co-incubation [41]. Besides, the hydrodynamic size and polydispersity index (PDI) of OMV/SaFeFA was measured by dissolving the nanoplatform in PBS supplemented with 10% FBS storage for 1 day and 7 days. The results are shown in Figure S3. On day 1, OMV/SaFeFA exhibited a size of 47.6 nm and a relatively narrow PDI of 0.301, indicating satisfactory dispersibility. After 7 days of storage, the size and PDI were 47.1 nm and 0.309, respectively. The minimal changes in size and PDI compared to the one-day storage results indicate excellent stability. Based on the analysis of X-ray photoelectron spectroscopic spectrum (Fig. 1e), both Fe^{2+} and Fe^{3+} were present in OMV/Fe. The element ratios of Fe^{2+} and Fe^{3+} were 72.17% and 27.83%, respectively (Fig. 1f). UV-vis absorption spectra showed that the SITNG agonist (SA)-loaded OMV particles (OMV/SaFA and OMV/SaFeFA) had the same characteristic peak as free SA solution (Fig. 1g), suggesting successful SA loading in OMV. Furthermore, we conducted zeta potential analysis of OMV with different modifications. As shown in Figure S4, OMV has a negative charge of −13.3 mV due to its negative-charged lipid substrates. The decreased electronegativity of OMV/Fe (−9.5 mV) compared to OMV implied the Fe ions were absorbed on the OMV. After DSPE-PEG-FA decoration, zeta potential of OMV changed to −18.5 mV from −13.3 mV, which arises from the negative-charged hydroxy groups in the DSPE-PEG-FA molecules. Furthermore, the higher potential of OMV/FeFA compared to OMV and OMV/FA suggested the Fe ions absorbed on the OMV/FA. Those results demonstrated the successful construction of the OMV/SaFeFA. Then, the pH responsive therapeutic release behaviors of OMV/SaFeFA were studied. The pH values at 7.4, 6.5, and 5.0 were set to stimulate physiological

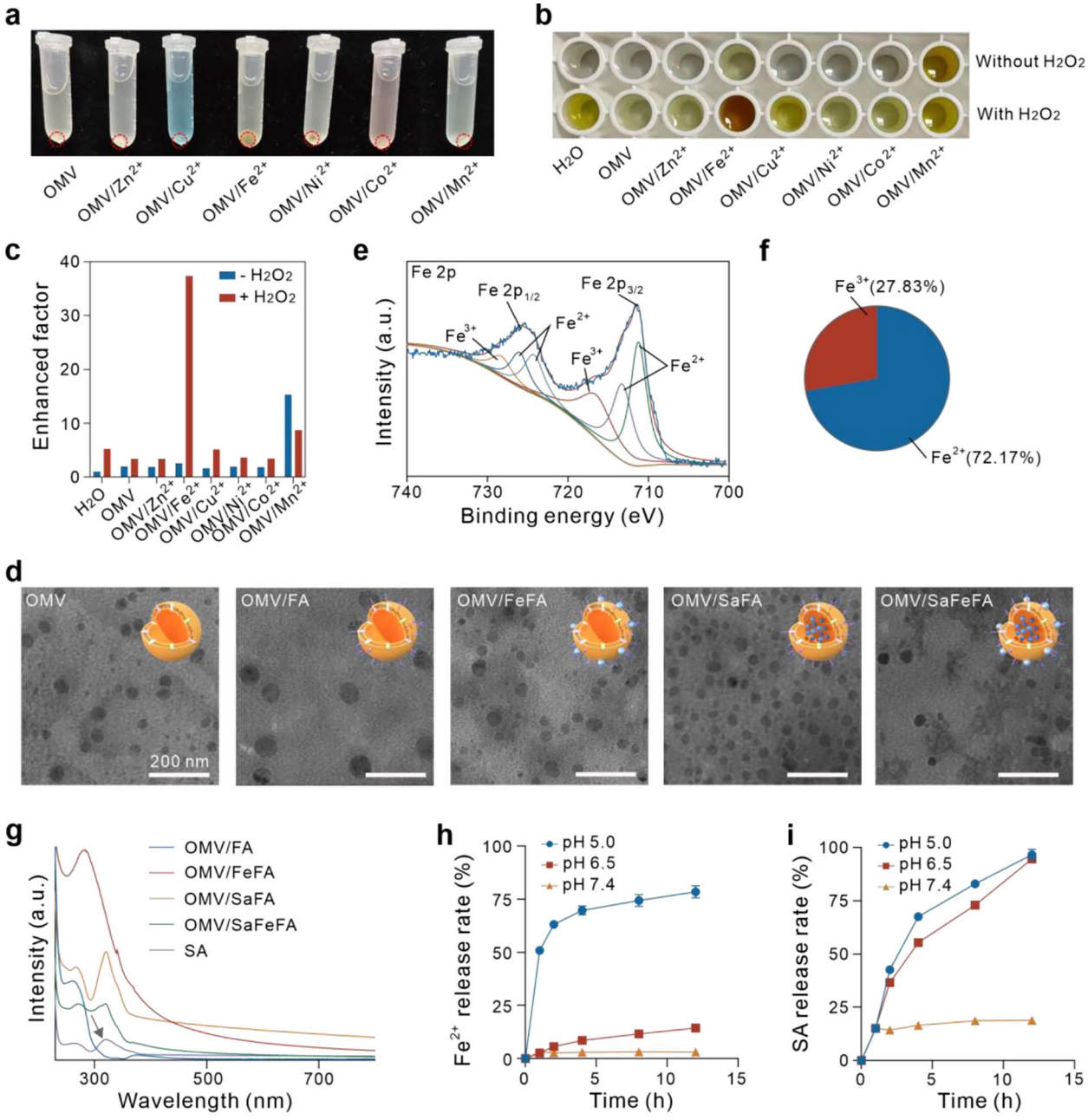

Fig. 1 (**a**) Photograph showing OMV incubated with various metal ions after centrifugation. The red dot cycle indicates the precipitate formed by OMV-ion interaction. (**b**) Photograph of TMB solution after incubating with indicated formulas for 10 min with or without H_2O_2 (50 μM). The reactions were terminated by adding equal volume of HCl (1 M) solution. (**c**) Enhanced factor of TMB absorbance at 450 nm compared to water with or without H_2O_2. (**d**) TEM images of OMV, OMV/FA, OMV/FeFA, OMV/SaFA, and OMV/SaFeFA. Scale bars are 200 nm. (**e**) The peak split of Fe 2p from X-ray photoelectron spectroscopic spectrum of OMV/Fe. (**f**) Percentage of Fe^{2+} and Fe^{3+} in OMV/Fe. (**g**) UV-vis spectra of OMV/SaFeFA during various modifications; the gray arrow indicates characteristic peak of SA (STING agonist-4). (**h, i**) Cumulative release percentage of Fe^{2+} (**h**) and STING agonist (**i**) under various pH values at different time points

environment, tumorous site, and lysosome, respectively. Under normal physiological environment, OMV/SaFeFA showed negligible release percentage of Fe^{2+} while the cumulative release percentage reached approximately 15% and 75% at pH 6.5 and 5.0, respectively, at 12 h (Fig. 1h). The moderate release of Fe^{2+} may hinge from the strong electrostatic interaction between iron cations and negative-charged OMV membrane. Similarly, there was minimal release of SA from OMV/SaFeFA at pH 7.4 (Fig. 1i). By contrast, SA rapidly release from OMV/SaFeFA under conditions of pH 6.5 and 5.0. The pH-responsive release of Fe^{2+} and SA was contributed to the

instability and fragility of OMV membranes [29], along with changes in permeability caused by protein conformational alterations [45, 46]. Therefore, the as-prepared OMV/SaFeFA nanoplatform exhibits excellent catalytic activity and pH-responsive therapeutic release property, demonstrating its potential in tumor-specific therapy.

In vitro anti-tumor effect of OMV/SaFeFA

Next, cellular experiments were conducted to assess the cellular uptake and cytotoxicity of OMV/FeFA. CY5 fluorescent molecules were loaded into OMV/FeFA through stirring, and flow cytometry was employed to evaluate the endocytosis of OMV/FeFA. As depicted in Fig. 2a, the fluorescence intensity of MC38 colon cancer cells was increased with incubating time, indicating that OMV/FeFA entered the MC38 cancer cells in a time-dependent manner. Afterward, the targeting-ability of FA was verified by incubating OMV/CY5FeFA with folate receptor-positive MC38 cells and folate receptor-negative 293T cells. Strong red fluorescent signals from confocal laser scanning microscope (CLSM) images were observed in MC38, while dim fluorescent signals were displayed in 293T cells, validating the active targeting ability of FA-modified OMV/CY5FeFA to MC38 cells (Figure S5). To assess cellular viability, MC38 cells were treated with OMV with various modifications for 24 h. As demonstrated in the CCK-8 assay (Fig. 2b), OMV/FA had negligible toxicity to cells, indicating excellent biocompatibility of the OMV/FA. By contrast, the viability of cells treated with OMV/FeFA decreased to approximately 68%, and STING agonist 4-loaded OMV/FA (OMV/SaFA) also exhibited moderate effects on cell viability. Notably, STING agonist 4/Fe^{2+}-loaded OMV (OMV/SaFeFA) demonstrated higher cellular killing ability than OMV/FeFA or OMV/SaFA, implying that STING agonist enhanced the therapeutic effects of OMV/FeFA. Besides, the cell killing capacity of OMV/SaFeFA was concentration-dependent, as demonstrated by the CCK-8 assay in Figure S6. A concentration of 7.5 μg/mL OMV/SaFeFA was sufficient to induce significant cell death, while 20 μg/mL OMV/SaFeFA reduced cell viability to approximately 28%, confirming the satisfactory killing capacity of OMV/SaFeFA against MC38 cells. Subsequently, the cell death mechanism was elucidated by adding various inhibitors including the ferroptosis inhibitor ferrostain-1 (Fer-1), the ROS scavenger vitamin E, and the autophagy inhibitor 3-methyladenine (3-MA). As illustrated in Fig. 2c, Fer-1 significantly abrogated OMV/SaFeFA-induced cell death, suggesting that OMV/SaFeFA induced cellular ferroptosis. Additionally, oxidation stress took part in OMV/SaFeFA-induced cell death, with autophagy serving as another major cell death mechanism in this process.

According to FerroOrange staining (Fig. 2d and S7), the concentration of Fe^{2+} in MC38 cells treated with OMV/SaFeFA increased with incubation time, further confirmed that the engineered OMV can efficiently deliver Fe^{2+} into cancer cells. The elevated Fe^{2+} levels will induce cellular ferroptosis through ROS generation. As shown in Fig. 2e, S8, and S9, Fe-decorated OMV/FeFA and OMV/SaFeFA significantly increased ROS levels in cancer cells, with the ROS signals notably higher in OMV/SaFeFA-treated cells in the presence of H_2O_2. Furthermore, the BboxiProbe O26 staining assay confirmed that the OMV/SaFeFA promoted $^{\bullet}OH$ generation in MC38 cells in the presence of H_2O_2 (Figures S10 and S11), providing further evidence of the potential of OMV/SaFeFA in tumor-specific catalytic therapy. As can be seen from Fig. 2f and S12, OMV/SaFeFA-treated cells displayed pronounced fluorescence signals, confirming cellular ferroptosis. Additionally, the Annexin V-FITC/PI staining assay demonstrated that OMV/SaFeFA induced cellular apoptosis (Figure S13), which may result from the elevated ROS levels.

Based on western blot investigation (Fig. 2g and S14a), there was an increased relative expression ratio of LC3II to LC3I in MC38 cells treated with OMV/SaFeFA, indicating the activation of cellular autophagy by OMV/SaFeFA. Additionally, as depicted in Figures S14b and S14c, OMV/SaFeFA treatment led to a decrease in the expression of FTH1 (ferritin heavy chain 1) and an increase in the expression of NCOA4 (nuclear receptor coactivator 4), which confirms that the induction of cellular ferritinophagy by OMV/SaFeFA [47]. The activated autophagy may originate from the pronounced oxidative stress and cellular damages in OMV/SaFeFA-treated cells. The degradation of FTH1 through ferritinophagy can increase the labile iron pool in cancer cells, thereby promoting cellular ferroptotic death [48, 49]. Furthermore, we investigated the activation of the STING pathway in dendritic cells (DCs). MC 38 cells were treated various formulations (PBS, OMV/FA, OMV/FeFA, OMV/SaFeFA, and OMV/SaFeFA), and their cell culture media were used to stimulate DC2.4 cells (see experimental details). We found that the expression of STING protein (Fig. 2h) and secreted IFN-β (Fig. 2i) were higher in group OMV/SaFeFA compared to the OMV/FeFA, OMV/SaFA, and other groups, suggesting that the activation of the STING pathway by OMV/SaFeFA in DC. Taken together, these results suggest that the as-prepared OMV/SaFeFA nanoplatform is able to induce cell ferroptosis through Fe^{2+} deliver and ROS generation while promoting STING activation in DCs.

As uncovered in many previous studies, oxidative stress, ferroptosis, and autophagy have been shown to induce calreticulin (CRT) exposure, thereby triggering antitumor immune responses. According to

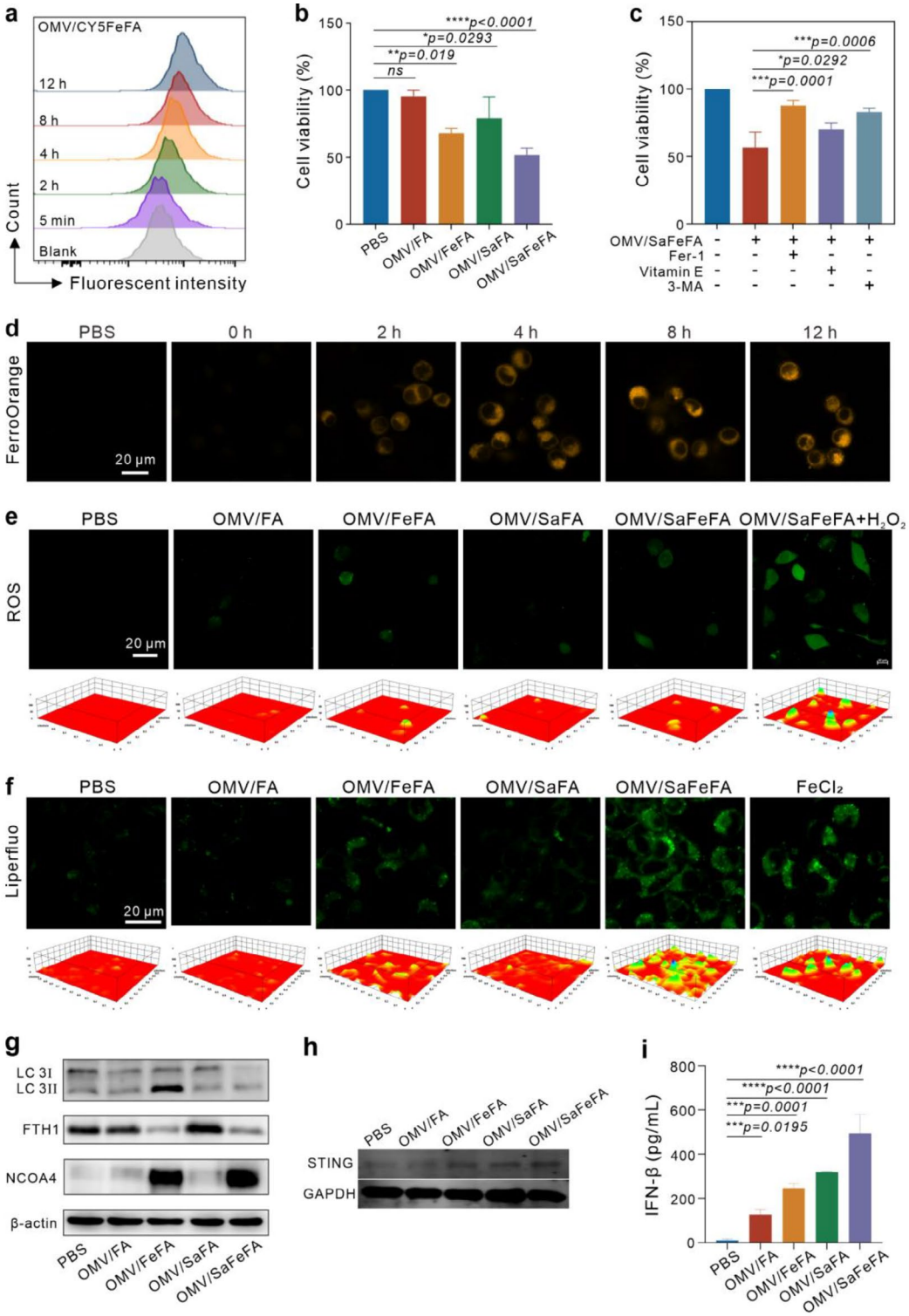

Fig. 2 (**a**) Internalization of MC38 cells treated with CY5-loaded OMV/FeFA was assessed by flow cytometric analysis at indicated time points. (**b**) Cell viability of MC38 cells treated with various formulations, $n = 5$. (**c**) Cell viability of MC38 cells treated with OMV/SaFeFA plus different kinds of inhibitors, $n = 5$. (**d-f**) Intracellular FerroOrange (**d**), ROS generation (**e**), and Liperfluo (**f**) of MC38 cells treated with different formulations. Scale bars are 20 μm. (**g, h**) Western blotting images of MC38 cells (**g**) and DC2.4 cells (**h**) treated with indicated formulations. (**i**) The secretion of IFN-β from the supernatant of DC2.4 cells with indicated treatments, $n = 3$. $^{**}P < 0.01$, $^{****}P < 0.0001$ and ns: not significant ($p > 0.05$), analyzed by one-way ANOVA, followed by Dunnett's multiple comparisons test. Data represent mean ± s.d

immunofluorescent staining assays (Figures S15 and S16), there were obvious fluorescence signals in MC38 cells treated with OMV/SaFeFA compared to those treated other formulations, indicating that the as-prepared OMV/SaFeFA induced CRT exposure. These findings underscore the potential of the OMV/SaFeFA nanoplatform to activate antitumor immune response.

Tumor-targeting ability of OMV/FA in vivo

The tumor accumulation capacity of drug delivery systems is critical for enhancing therapeutic effects and subsequent antitumor immune responses. Thus, we investigated the biodistribution of engineered OMV by loading of fluorescent cyanine 5 (CY5) molecules and PEGylation with DSPE-PEG (referred to as OMV/CY5-PEG) or DSPE-PEG-FA (referred to OMV/CY5-PEG-FA). In a colon tumor model, nine MC38 tumor-bearing C57/BL6 mice were randomly divided into three groups. Mice were received intravenous injection (i.v.) of CY5, OMV/CY5-PEG, and OMV/CY5-PEG-FA. Subsequently, fluorescent images and signals were recorded using an IVIS system at various time points post-injection (20 min, 2 h, 4 h, 8 h, 10 h, and 24 h) (Fig. 3a). As depicted in Fig. 3b and c, minimal fluorescence signals were observed at tumor sites following administration of free CY5. On the contrary, mice treated with OMV/CY5-PEG exhibited strong fluorescence signals at tumor sites, indicating enhanced tumor targeting of CY5 molecules by OMV. Remarkably, mice injected with OMV/CY5-PEG-FA showed significantly higher fluorescence intensity compared to those treated with free CY5 and OMV/CY5-PEG. After 24 h, mice were euthanized, their tumors and major organs (heart, liver, spleen, lung, and kidney) were collected and imaged. As can be seen from Fig. 3d and e, fluorescence signals of tumor in OMV/CY5-PEG-FA-treated mice were markedly higher than in other two groups, further demonstrating PEGylation of OMV with DSPE-PEG-FA enhanced the tumor-targeting of the OMV. Additionally, in a breast tumor (4T1)-bearing mouse model, OMV/CY5-PEG-FA also exhibited superior tumor targeting compared to free CY5 and OMV/CY5-PEG based on tissue imaging (Figures S17) and CLSM images of tumor slices (Figures S18). These findings provide further evidence that DSPE-PEG-FA-decorated OMV has excellent tumor-targeting capacity, and it suggests that the fabricated OMV/SaFeFA with potential in tumor-targeted therapy.

The antitumor effect of OMV/SaFeFA

Next, we further assessed the therapeutic effects and antitumor immune response stimulation of the engineered OMV/SaFeFA in a mouse colon tumor model. Initially, 1×10^6 MC38 cells were subcutaneously injected into the right hind leg flank of C57/BL6 mice. Upon the tumors reaching about 200 mm^3 in size, twenty-five tumor-bearing mice were randomly divided into five groups and injected with PBS, OMV/FA, OMV/FeFA, OMV/SaFA, and OMV/SaFeFA *via* the tail vein. Subsequently, tumor size and body weight were monitored every two days (Fig. 4a). As shown in Fig. 4b, tumors in PBS-treated mice grew rapidly, whereas those in OMV/FA-treated mice showed some degree of inhibition. This inhibition is likely due to the OMV's ability to activate the immune response, primarily through its lipopolysaccharide component, which is consistent with previous reports [30, 43]. OMV/FeFA displayed slightly slower tumor growth compared to OMV/FA. Notably, both the OMV/SaFA and OMV/SaFeFA groups significantly suppressed tumor development. Specifically, tumor volumes on day 16 in the OMV/SaFeFA group were the smallest among all groups (Figure S19), indicating excellent therapeutic efficacy in tumor control. On day 16, mice were euthanized for ex vivo inspection of tumor weight inhibition rate and photographed (Fig. 4c and d), which further supporting the excellent therapeutic effects of the as-prepared OMV/SaFeFA. The tumor weight inhibitory rate of OMV/SaFeFA was 77.6% (Fig. 4e). As shown in Fig. 4f, there was no obvious difference in body weights of mice treated with various formulations. Moreover, blood biochemical parameters (Figure S20 and Table S1) and hematoxylin and eosin (H&E) histological staining of major organs (Figure S21) of mice that received various treatments showed no notable changes compared to PBS-treated group. These results indicate that OMV/SaFeFA holds excellent biocompatibility. Survival analysis revealed that tumor-bearing mice treated with OMV/SaFeFA had superior survival rate (66.3% at day 58) compared to those treated with other groups (Fig. 4g). Subsequently, the therapeutic mechanisms were studied (Fig. 4h). As can be seen from histological H&E and terminal deoxynucleotidyl transferase dUTP nick end labeling (TUNEL) staining of tumor slices, OMV/SaFeFA induced pronounced cell damages compared to the other groups. OMV and STING activation contributes to IFN-γ production whereby inhibiting the expression of SLC7A11. Thereafter, we detected the IFN-γ levels in tumors by immunohistochemistry (IHC) staining of tumor slices and in serum using commercial kits. Unsurprisingly, we found that OMV/SaFeFA enhanced the secretion of IFN-γ in tumor-bearing mice (Fig. 4h and S22). Additionally, the expression of SLC7A11 in tumors was significantly suppressed by OMV/SaFeFA. Functionally, SLC7A11 acts as a cystine/glutamate antiporter for cystine uptake for GSH synthesis, which mitigates oxidative stress and ferroptosis. Besides, GSH serves as a cofactor of GPX4, an anti-ferroptosis enzyme. Thus, the inhibition of SLC7A11 by IFN-γ induced by OMV/SaFeFA led to decreased GPX4, as confirmed by IHC

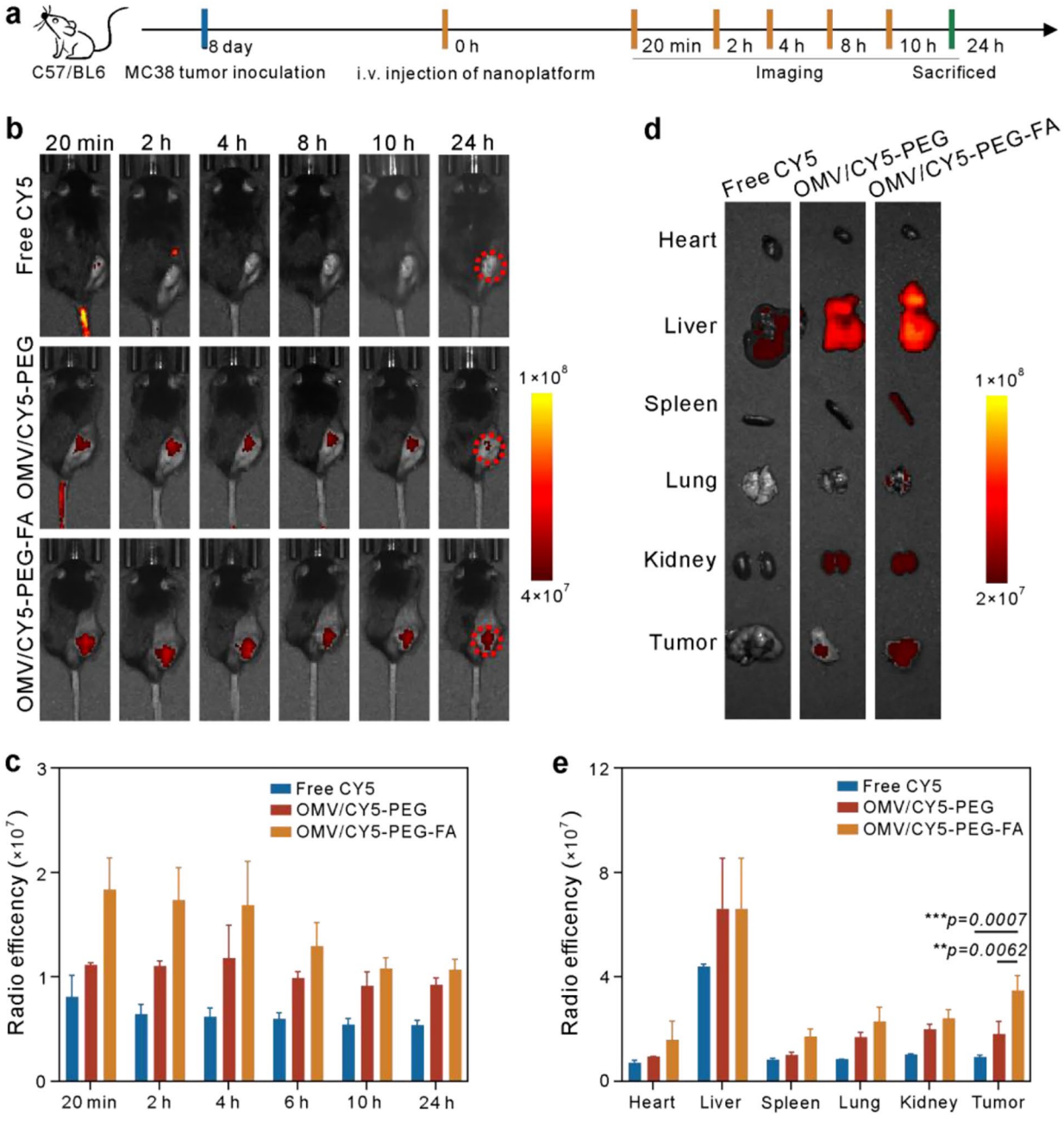

Fig. 3 In vivo fluorescence imaging of MC 38 tumor-bearing mice after i.v. injection of different formulations. (**a**) Treatment process. (**b, c**) Representative fluorescence images (**b**) and corresponding statistical fluorescent intensity (**c**) of mice at various time points after injection of free CY5, OMV/CY5-PEG, and OMV/CY5-PEG-FA at different time points, $n = 3$; tumor sites are indicated by red dots. (**d, e**) Representative fluorescence images (**d**) and quantification of fluorescent intensity (**e**) of tumors and major organs 24 h post-injection of free CY5, OMV/CY5-PEG, and OMV/CY5-PEG-FA, $n = 3$. $^{**}P < 0.01$, $^{****}P < 0.0001$ and ns: not significant ($p > 0.05$), analyzed by one-way ANOVA, followed by Dunnett's multiple comparisons test. Data represent mean ± s.d

staining of tumor slices. Additionally, in vivo ferroptosis visualization was further confirmed by the immunohistochemical staining of FTH1 and NCOA4 proteins. As shown in Figure S23, OMV/SaFeFA treatment decreased FTH1 expression and increased NCOA4 expression, mirroring the in vitro ferroptosis analysis results in Fig. 2g. As a matter of fact, these findings suggest that the as-prepared OMV/SaFeFA can induce tumor ferroptosis by inhibiting SLC7A11, FTH1, and GPX4, while maintaining excellent biocompatibility.

Finally, we investigated the antitumor immune responses of MC38 tumor-bearing mice following various treatments. On day 16, mice were euthanized, and their tumors were collected. Subsequently, tumor

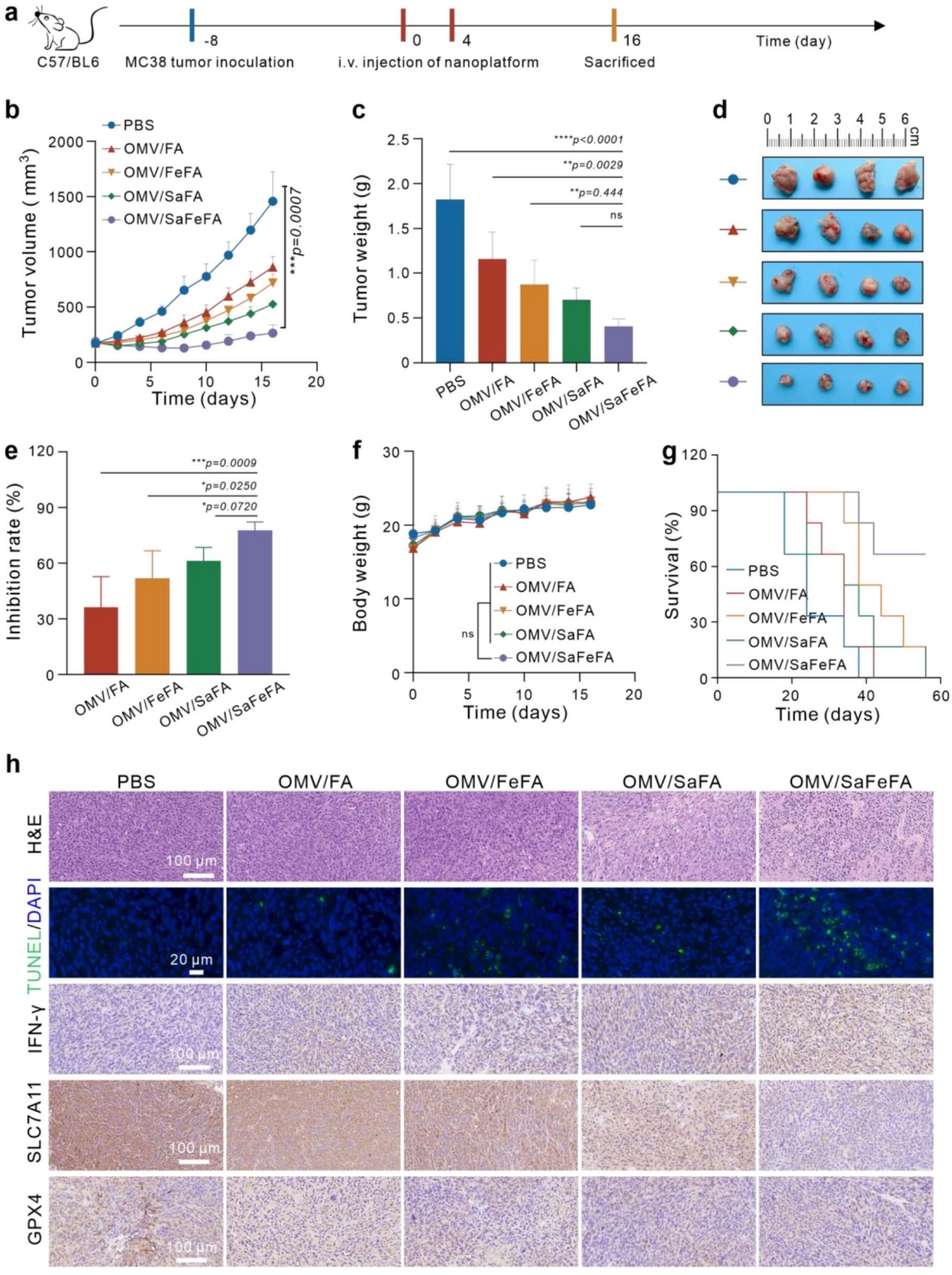

Fig. 4 In vivo tumor therapy. (**a**) Treatment process. (**b**) Tumor growth curves of MC38 tumor-bearing mice during the period of different treatments. (**c, d**) Tumor weights (**c**) and the corresponding photograph (**d**) of tumors from mice received various treatments on day 16. (**e**) Tumor weight inhibition rate of mice after treatment. (**f**) Body weight monitoring of mice during the period of various treatments. (**g**) Survival percentage of MC38 tumor bearing mice received indicated treatments. (**h**) Representative images of H&E staining, TUNEL staining, and immunohistochemical staining of the IFN-γ, SLC7A11, and GPX4 of tumor slices from MC38 tumor bearing mice received various treatments on day 16. $^{**}P < 0.01$, $^{****}P < 0.0001$ and ns: not significant ($p > 0.05$), analyzed by one-way ANOVA, followed by Dunnett's multiple comparisons test. Data represent mean ± s.d

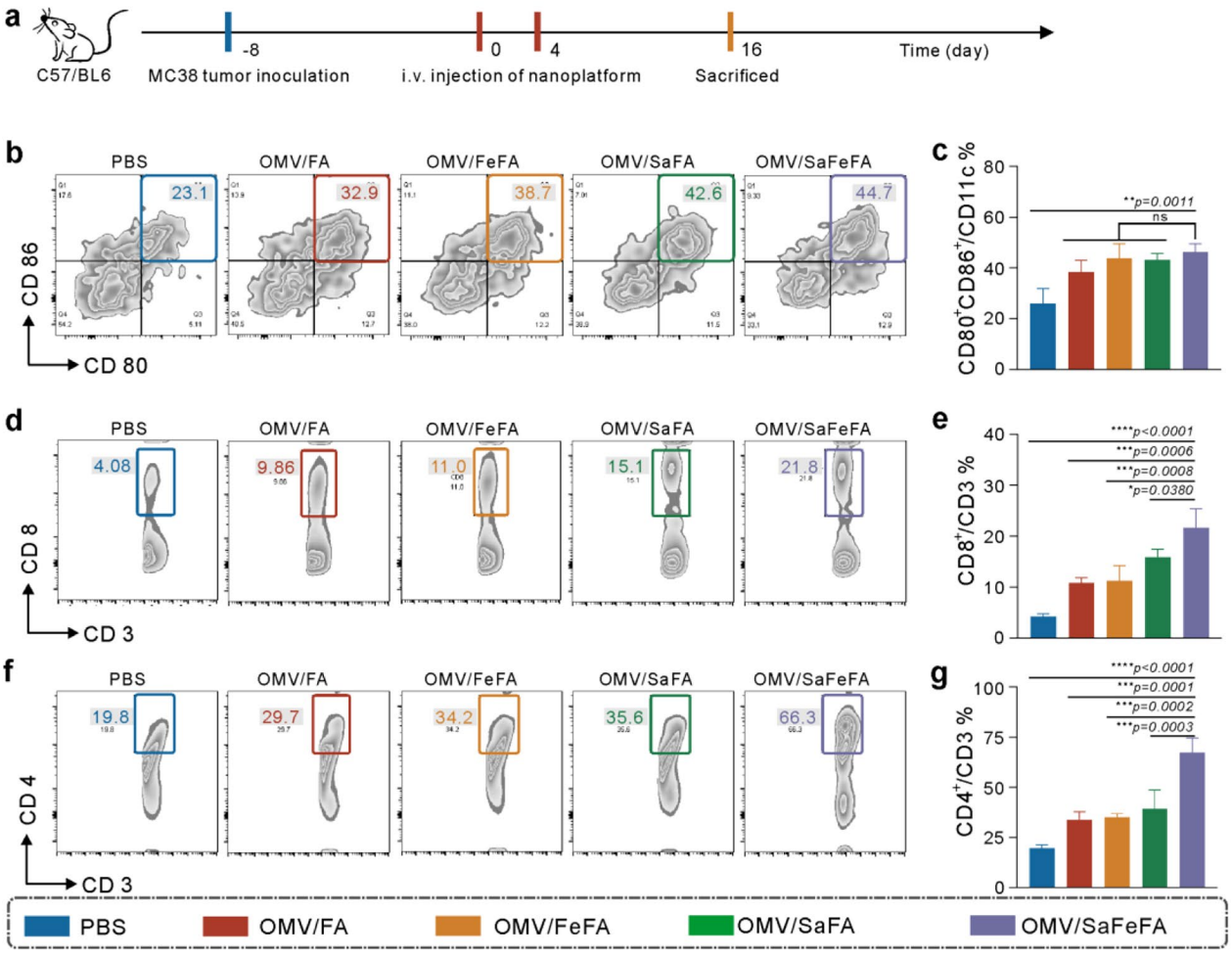

Fig. 5 The mechanism of antitumor immunity responses. (**a**) Treatment process. (**b, c**) Representative flow cytometric images (**b**) and statistical results (**c**) of DC maturation (gated on $CD11c^+CD80^+CD86^+$) in tumors. (**d, e**) Representative flow cytometric images (**d**) and statistical results (**e**) of $CD8^+$ T cells in tumors. (**f, g**) Representative flow cytometric images (**f**) and statistical results (**g**) of $CD4^+$ T cells in tumors. $^{**}P < 0.01$, $^{****}P < 0.0001$ and ns: not significant ($p > 0.05$), analyzed by one-way ANOVA, followed by Dunnett's multiple comparisons test. Data represent mean ± s.d

tissues were then processed to single-cell suspensions and stained with fluorescent antibodies according to the manufacturer's protocols (Experiment section). Flow cytometric analysis of DCs, cytotoxic T lymphocytes ($CD8^+$ T cells), and helper T cells ($CD4^+$ T cells) was illustrated in Fig. 5, with their gating strategies outlined in Figure S24. According to quantitative analysis and comparison, Fe ion or STING agonist-4 functionalization of OMV/FA enhanced DC maturation, while OMV/SaFeFA induced maturation of a greater number of DCs (Fig. 5b, c). Furthermore, intratumoral levels of $CD8^+$ T cells (Fig. 5d, e) and $CD4^+$ T cells (Fig. 5f, g) were significantly elevated by OMV/SaFeFA compared to other formulations. Collectively, OMV/SaFeFA elicited robust antitumor immune responses, achieving substantial therapeutic efficacy through a combination of ferroptosis and immunotherapy.

Conclusion

In summary, we present a novel biological nanovector for tumor synergistic ferroptosis-immunotherapy by rationally functionalizing bacteria-derived OMV with ferrous ions, a STING agonist, and tumor-targeting DSPE-PEG-FA molecules. The as-prepared OMV/SaFeFA platform efficiently delivers ferrous ions to cancer cells, inducing cancer cell ferroptosis through oxidative stress and autophagy, while also activating the STING pathway in DCs. Remarkable tumor inhibiting and survival rates in colon tumor-bearing mice demonstrated the significant therapeutic potential of OMV/SaFeFA. Mechanism analyses reveal that OMV/SaFeFA suppresses the expression of SLC7A11 and GPX4 by promoting the IFN-γ production, with robust antitumor immune responses including DC maturation, and increased levels of intratumoral $CD8^+$ and $CD4^+$ T cells. On bases of its conspicuous biocompatibility and therapeutic efficacy, OMV/SaFeFA

represents a promising platform for the next-generation tumor treatment.

Supplementary Information

The online version contains supplementary material available at https://doi.org/10.1186/s12951-024-02747-3.

Supplementary Material 1

Acknowledgements
This work was supported by the key Clinical Specialty Discipline Construction Program of Fuzhou, Fujian, P.R.C (20230105), and Fuzhou Science and Technology Plan Project (2023-S-021), the National Natural Science Foundation of China (62275048 and 32201153), and the Science and Technology Planning Project of Fujian Province (2021J05031 and 2023J01292).

Author contributions
Ying Sun: Writing - original draft, Methodology, Investigation. Funding acquisition Yan-Yan Ma: Writing, Investigation. Shijie Shangguan: Writing, Investigation. Yihang Ruan: Writing, Investigation. Huimei Cai: Writing - review & editing, Project administration. Shuangqian Yan: Writing - review & editing, Supervision, Project administration, Funding acquisition, Conceptualization. All authors participated in results discussion.

Data availability
No datasets were generated or analysed during the current study.

Declarations

Competing interests
The authors declare no competing interests.

Received: 25 May 2024 / Accepted: 2 August 2024
Published online: 09 August 2024

References

1. Dixon SJ, Lemberg KM, Lamprecht MR, Skouta R, Zaitsev EM, Gleason CE, Patel DN, Bauer AJ, Cantley AM, Yang WS. Ferroptosis: an iron-dependent form of nonapoptotic cell death. Cell. 2012;149:1060–72.
2. Pope LE, Dixon SJ. Regulation of ferroptosis by lipid metabolism. Trends Cell Biol. 2023;28:2843–56.
3. Lei G, Zhuang L, Gan B. Targeting ferroptosis as a vulnerability in cancer. Nat Rev Cancer. 2022;22:381–96.
4. Chen X, Kang R, Kroemer G, Tang D. Broadening horizons: the role of ferroptosis in cancer. Nat Rev Clin Oncol. 2021;18:280–96.
5. Li J, Cao F, Yin H-l, Huang Z-j, Lin Z-t, Mao N, Sun B, Wang G. Ferroptosis: past, present and future. Cell Death Dis. 2020;11:88.
6. Kang N, Son S, Min S, Hong H, Kim C, An J, Kim JS, Kang H. Stimuli-responsive ferroptosis for cancer therapy. Chem Soc Rev. 2023;52:3955–72.
7. Yang H, Yao X, Liu Y, Shen X, Li M, Luo Z. Ferroptosis nanomedicine: clinical challenges and opportunities for modulating tumor metabolic and immunological landscape. ACS Nano. 2023;17:15328–53.
8. Yang WS, SriRamaratnam R, Welsch ME, Shimada K, Skouta R, Viswanathan VS, Cheah JH, Clemons PA, Shamji AF, Clish CB. Regulation of ferroptotic cancer cell death by GPX4. Cell. 2014;156:317–31.
9. Badgley MA, Kremer DM, Maurer HC, DelGiorno KE, Lee H-J, Purohit V, Sagalovskiy IR, Ma A, Kapilian J, Firl CE. Cysteine depletion induces pancreatic tumor ferroptosis in mice. Science. 2020;368:85–9.
10. Wang W, Green M, Choi JE, Gijón M, Kennedy PD, Johnson JK, Liao P, Lang X, Kryczek I, Sell A. CD8$^+$ T cells regulate tumour ferroptosis during cancer immunotherapy. Nature. 2019;569:270–4.
11. Zhao L, Zhou X, Xie F, Zhang L, Yan H, Huang J, Zhang C, Zhou F, Chen J, Zhang L. Ferroptosis in cancer and cancer immunotherapy. Cancer Commun. 2022;42:88–116.
12. Sun L-L, Linghu D-L, Hung M-C. Ferroptosis: a promising target for cancer immunotherapy. Am J Cancer Res. 2021;11:5856.
13. Zhang X, Ge H, Ma Y, Song L, Ma Y, Tian G, Wang L, Meng Q, Sun X. Engineered anti-cancer nanomedicine for synergistic ferroptosis-immunotherapy. Chem Eng J. 2023;455:140688.
14. Ruan Y, Zhuang H, Zeng X, Lin L, Wang X, Xue P, Xu S, Chen Q, Yan S, Huang W. Engineered microbial nanohybrids for tumor-mediated NIR II photothermal enhanced ferroptosis/cuproptosis and immunotherapy. Adv Healthc Mater. 2024;13:2302537.
15. Shen Z, Song J, Yung BC, Zhou Z, Wu A, Chen X. Emerging strategies of cancer therapy based on ferroptosis. Adv Mater. 2018;30:1704007.
16. Liang C, Zhang X, Yang M, Dong X. Recent progress in ferroptosis inducers for cancer therapy. Adv Mater. 2019;31:1904197.
17. Xue P, Zhuang H, Bai T, Zeng X, Deng J, Shao S, Yan S. Iron (II)-based metal-organic framework nanozyme for boosting tumor ferroptosis through inhibiting DNA damage repair and system Xc. J Nanobiotechnol. 2024;22:228.
18. Li W, Liu S, Ding H, Zhao R, Zang P, Li S, Fang L, Li R, Zhang M, Yang P. Three-step depletion strategy of glutathione: tunable metal-organic-framework-engineered nanozymes for driving oxidative/nitrative stress to maximize ferroptosis therapy. Nano Lett. 2024;24:2071–80.
19. Zhang Y, Chen P-H, Li B, Guo H, Zhu J, Dang Z, Lei S, Huang P, Lin J. Comprehensively optimizing fenton reaction factors for antitumor chemodynamic therapy by charge-reversal theranostics. ACS Nano. 2023;17:16743–56.
20. Yang B, Chen Y, Shi J. Nanocatalytic medicine. Adv Mater. 2019;31:1901778.
21. Tang G, He J, Liu J, Yan X, Fan K. Nanozyme for tumor therapy: Surface modification matters, Exploration (2021) 75–89.
22. Zeng X, Ruan Y, Chen Q, Yan S, Huang W. Biocatalytic cascade in tumor microenvironment with a Fe_2O_3/Au hybrid nanozyme for synergistic treatment of triple negative breast cancer. Chem Eng J. 2023;452:138422.
23. Zhuang H, Xue P, Shao S, Zeng X, Yan S. In situ generation of hybrid alginate hydrogels for enhanced breast tumor ferrotherapy through multiplex magnifying redox imbalances. Int J Biol Macromol. 2024;258:128952.
24. Zhu Y, Gong P, Wang J, Cheng J, Wang W, Cai H, Ao R, Huang H, Yu M, Lin L. Amplification of lipid peroxidation by regulating cell membrane unsaturation to enhance chemodynamic therapy. Angew Chem. 2023;135:e202218407.
25. Hou M, Liu M, Yu H, Kou Y, Jia J, Zhou Q, Zhang F, Zhao D, Zhao T, Li X. Spatially asymmetric nanoparticles for boosting ferroptosis in tumor therapy. Nano Lett. 2024;24:1284–93.
26. Liu J, Zhan J, Zhang Y, Huang L, Yang J, Feng J, Ding L, Shen Z, Chen X. Ultrathin clay nanoparticles-mediated mutual reinforcement of ferroptosis and cancer immunotherapy. Adv Mater. 2023;36:2309562.
27. Wang G, Xie L, Li B, Sang W, Yan J, Li J, Tian H, Li W, Zhang Z, Tian Y. A nanounit strategy reverses immune suppression of exosomal PD-L1 and is associated with enhanced ferroptosis. Nat Commun. 2021;12:1–12.
28. Liu Y, Niu R, Deng R, Song S, Wang Y, Zhang H. Multi-enzyme co-expressed dual-atom nanozymes induce cascade immunogenic ferroptosis *via* activating interferon-γ and targeting arachidonic acid metabolism. J Am Chem Soc. 2023;145:8965–78.
29. Kim OY, Dinh NTH, Park HT, Choi SJ, Hong K, Gho YS. Bacterial protoplast-derived nanovesicles for tumor targeted delivery of chemotherapeutics. Biomaterials. 2017;113:68–79.
30. Zhuang W-R, Wang Y, Nie W, Lei Y, Liang C, He J, Zuo L, Huang L-L, Xie H-Y. Bacterial outer membrane vesicle based versatile nanosystem boosts the efferocytosis blockade triggered tumor-specific immunity. Nat Commun. 2023;14:1675.
31. Feng J, Xiu Q, Huang Y, Troyer Z, Li B, Zheng L. Plant derived vesicle-like nanoparticles as promising biotherapeutic tools: present and future. Adv Mater. 2023;35:2207826.
32. Kim OY, Park HT, Dinh NTH, Choi SJ, Lee J, Kim JH, Lee S-W, Gho YS. Bacterial outer membrane vesicles suppress tumor by interferon-γ-mediated antitumor response. Nat Commun. 2017;8:1–9.
33. Gujrati V, Kim S, Kim S-H, Min JJ, Choy HE, Kim SC, Jon S. Bioengineered bacterial outer membrane vesicles as cell-specific drug-delivery vehicles for cancer therapy. ACS Nano. 2014;8:1525–37.
34. Liu G, Ma N, Cheng K, Feng Q, Ma X, Yue Y, Li Y, Zhang T, Gao X, Liang J. Bacteria-derived nanovesicles enhance tumour vaccination by trained immunity. Nat Nanotechnol. 2023;19:1–12.
35. Suri K, D'Souza A, Huang D, Bhavsar A, Amiji M. Bacterial extracellular vesicle applications in cancer immunotherapy. Bioact Mater. 2023;22:551–66.
36. Zheng K, Feng Y, Li L, Kong F, Gao J, Kong X. Engineered bacterial outer membrane vesicles: a versatile bacteria-based weapon against gastrointestinal tumors. Theranostics. 2024;14:761–87.
37. Nie W, Jiang A, Ou X, Zhou J, Li Z, Liang C, Huang L-L, Wu G, Xie H-Y. Metal-polyphenol prison attenuated bacterial outer membrane vesicle

for chemodynamics promoted *in situ* tumor vaccines. Biomaterials. 2024;304:122396.
38. Chen X, Li P, Luo B, Song C, Wu M, Yao Y, Wang D, Li X, Hu B, He S. Surface mineralization of engineered bacterial outer membrane vesicles to enhance tumor photothermal/immunotherapy. ACS Nano. 2024;18:1357–70.
39. Leventhal DS, Sokolovska A, Li N, Plescia C, Kolodziej SA, Gallant CW, Christmas R, Gao J-R, James MJ. Abin-Fuentes, immunotherapy with engineered bacteria by targeting the STING pathway for anti-tumor immunity. Nat Commun. 2020;11:2739.
40. Van Herck S, Feng B, Tang L. Delivery of STING agonists for adjuvanting subunit vaccines. Adv Drug Deliver Rev. 2021;179:114020.
41. Guo Q, Li X, Zhou W, Chu Y, Chen Q, Zhang Y, Li C, Chen H, Liu P, Zhao Z. Sequentially triggered bacterial outer membrane vesicles for macrophage metabolism modulation and tumor metastasis suppression. ACS Nano. 2021;15(8):13826–38.
42. Hong S, Zhang Q-L, Zheng D-W, Zhang C, Zhang Y, Ye J-J, Cheng H, Zhang X-Z. Enzyme mimicking based on the natural melanin particles from human hair. iScience. 2020;23:100778.
43. Kim OY, Park HT, Dinh NTH, Choi SJ, Lee J, Kim JH, Lee S-W, Gho YS. Bacterial outer membrane vesicles suppress tumor by interferon-γ-mediated antitumor response. Nat Commun. 2017;8:626.
44. Ahmed AAQ, Besio R, Xiao L, Forlino A. Outer membrane vesicles (OMVs) as biomedical tools and their relevance as immune-modulating agents against H. Pylori infections: current status and future prospects. Int J Mol Sci. 2023;24:8542.
45. de Oliveira LC, da Silva VM, Colussi F, Cabral AD, de Oliveira Neto M, Squina FM, Garcia W. Conformational changes in a hyperthermostable glycoside hydrolase: enzymatic activity is a consequence of the loop dynamics and protonation balance. PLoS ONE. 2015;10:e0118225.
46. Ludwiczek ML, D'Angelo I, Yalloway GN, Brockerman JA, Okon M, Nielsen JE, Strynadka NC, Withers SG, McIntosh LP. Strategies for modulating the pH-dependent activity of a family 11 glycoside hydrolase. Biochemistry. 2013;52:3138–56.
47. Mancias JD, Wang X, Gygi SP, Harper JW, Kimmelman AC. Quantitative proteomics identifies NCOA4 as the cargo receptor mediating ferritinophagy. Nature. 2014;509:105–9.
48. Gao M, Monian P, Pan Q, Zhang W, Xiang J, Jiang X. Ferroptosis is an autophagic cell death process. Cell Res. 2016;26:1021–32.
49. Hou W, Xie Y, Song X, Sun X, Lotze MT, Zeh HJ III, Kang R, Tang D. Autophagy promotes ferroptosis by degradation of ferritin. Autophagy. 2016;12:1425–8.

Publisher's Note